ICAS 2021 SHANGHAI
International Council of the Aeronautical Sciences
32nd Congress of the International Council of the Aeronautical Sciences
September 6-10, 2021
Pudong Shangri-La, Shanghai, China

TURBINE STRUCTURE ANALYSIS AND IMPROVEMENT OF A HIGH-SPEED ROTOR WITH MULTI-DISK AND MULTI-SUPPORT

NIE Wei-jian [1,2], DENG Wang-qun [1,2], CHEN Ya-nong [1,2] & ZOU-Lei [1]

[1] AECC Hunan Aviation Powerplant Research Institute, Zhuzhou, China
[2] Key Laboratory of Aero engine Vibration Technology, Aero Engine Corporation of China, Zhuzhou, China

Abstract

Taking a simulated low-pressure rotor of a small turbofan engine as the study object, the study analyzed the causes of vibration faults that appeared in the process of dynamic characteristic experiment of the rotor. Besides, structure improvement measures of the turbine were put forward and test verifications were carried out on the high-speed rotating test rig. Finite element analysis model of the rotor was established, the first three stages critical speeds and vibration shapes were obtained. The results showed that the rotor could operate to the rated working speed after the improvement of turbine structure. The model well reflects the dynamic characteristic of the rotor. This study solves a key technology in the engine development, it also provided references for structure design of the true low-pressure rotor of engine and rotors of the same type.

Keywords: Aero-engine; High Speed Flexible Rotor; Vibration Fault; Structure Improve; Test Verification

1. Introduction

Rotor is a very important part of aeroengine. At the stage of scheme design, it is often necessary to verify the rationality of rotor structure design through test and analysis. Wu Guofan carried out the dynamic characteristics' analysis and experimental research on a gas generator rotor [1]. Deng Wangqun analyzed the influence of support stiffness and axial position on the critical speeds of a low-pressure rotor in a type engine, which provided a theoretical basis for support structure and layout [2]. However, there are often a variety of faults in the process of test. Rotor fault is an important cause of vibration fault appearing in engine. Therefore, it is of great significance to study the rotor fault. Many scholars have carried out theoretical and experimental research on fault diagnosis and troubleshooting methods. The fault diagnosis method of high-pressure rotor vibration of aeroengine was studied systematically by Gao Feng [3]. Liu Jianxiong established a coupled vibration fault analysis model for the specific structure of an aeroengine rotor [4]. Huang Guoyuan conducted in-depth simulation and Experimental Research on the vibration fault of rotor system caused by unbalance, misalignment and friction[5].Liu Yang established the mechanical model and finite element model of the rotor system with two disks misalignment rubbing coupling faults, and obtained the dynamic characteristics of the rotor system misalignment rubbing coupling fault, which provided a basis for judging the faults [6]. Xu Qi studied the coupling fault quantitative diagnosis method of multi span rotor system, and verified by experiment that this method has good applicability to the main vibration faults of the rotor system [7]. Deng Wangqun put forward troubleshooting measures for the instability and vibration exceeding limit value fault of a small turbofan engine at high speed during the test, which has been verified by the test [8].

The simulated low-pressure rotor of a small turbofan engine was a high-speed flexible rotor with multi disk and multi support. In this paper, the vibration fault of the rotor in the test process was studied, the causes of the fault were analyzed, and the improvement measures were taken. Besides, structure improvement measures of the turbine were put forward and test verifications were carried out on the high-speed rotating test rig. The vibration fault was successfully eliminated finally. This study solved a key technology in the engine development, it also provided references for structure design of the true low-pressure rotor of engine and rotors of the same type.

2. Structure of the Rotor

The structure of the simulated low-pressure rotor is as shown in figure 1. The rotor was mainly composed of five stimulated disks, including fan simulated disks, one booster stage simulated disk and turbine simulated disks, and low-pressure shaft with integral solid structure. There were four bearings in the rotor, among which the No.1 bearing was ball bearing, the No.2, No.5 and No.6 bearings were all roller bearing. No.1 support adopted squirrel cage type elastic support, No.5 support adopted elastic ring type elastic support, No.2 and No.6 supports were all rigid supports.
The high-speed flexible rotor, with complex structure, having four supports with 0-3-1 bearing scheme, was characteristic of multi-disk, multi-support and high rated working speed.

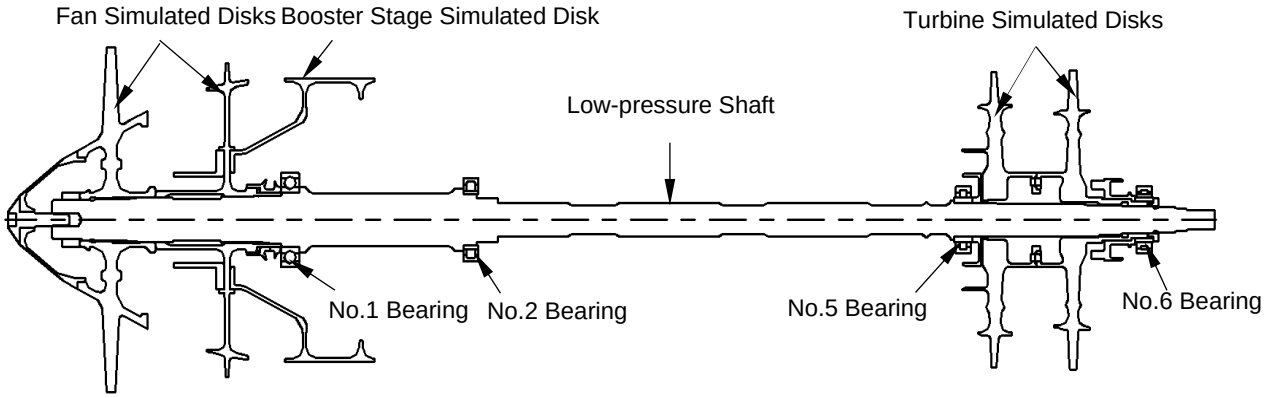

Figure 1 – Structural sketch of the simulated low-pressure rotor.

3. Fault Analysis and Structure Improvement

The installation and test schematic diagram of the simulated low-pressure rotor on the test rig is shown in Figure 2. The dynamic characteristic test of the rotor was carried out on the high-speed rotating test rig. The power input was realized through the connection of a slender floating shaft. During the test, the deflection of the rotor and the vibration acceleration of the pedestals were measured. The displacement sensors were arranged at positions ①, ② and ③ as shown in figure 2 to measuring the deflection of the rotor. The displacement sensors D_1 and D_2 were arranged at vertical direction of positions ① and ③ respectively, and D_3 and D_4 were arranged at vertical and horizontal direction of position② respectively. Two vibration acceleration sensors were arranged on each pedestal to measuring the vibration accelerations. In figure 2, "⊥" and "=" indicate the vertical and horizontal directions of measurement respectively.
The installation photo of the simulated low-pressure rotor on the test rig is shown in Figure 3.

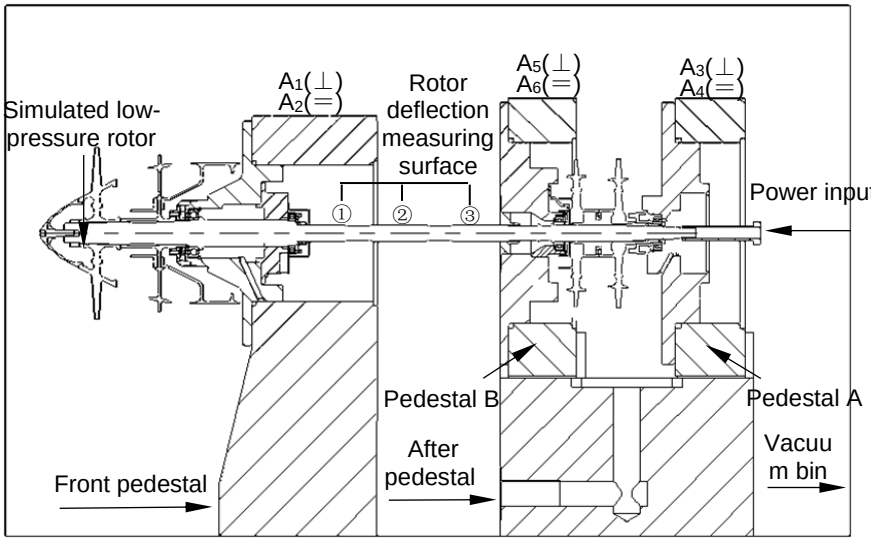

Figure 2 – Installation and test schematic diagram of the simulated low-pressure rotor.

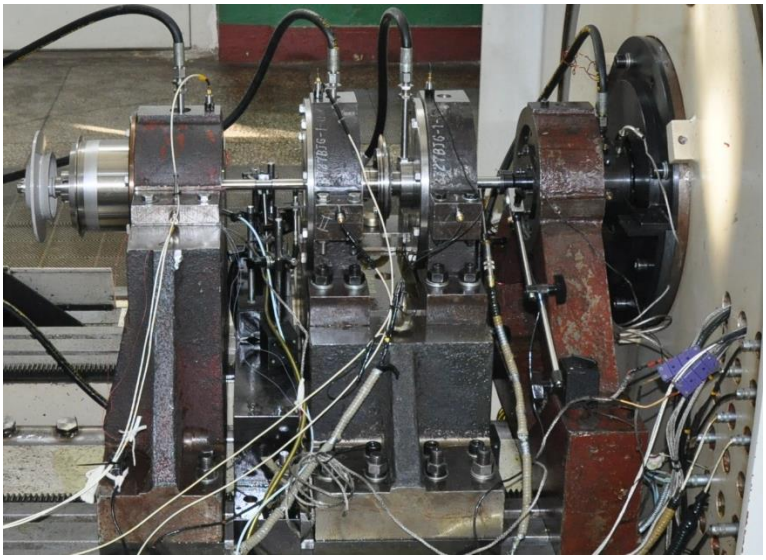

Figure 3 – Installation photo of the simulated low-pressure rotor.

3.1 Fault Phenomenon

When the rotor was running to 40 percent rated working speed, the vibration acceleration measured by A_6 sensor achieved 5.8g which exceeded the limit value. Meanwhile, as it increased sharply with the increase of rotational speed, the test was in no security.

The frequency spectrum of vibration accelerations of each pedestal at 40 percent rated working speed is shown as figure 4. The results of spectrum analysis showed that the value of the base frequency was small, there was non-integer frequency like 2.4 times, 3.2 times and 3.4 times, the frequency component was very complex. And the 3.2 times frequency was the main frequency component which caused vibration acceleration transfinite.

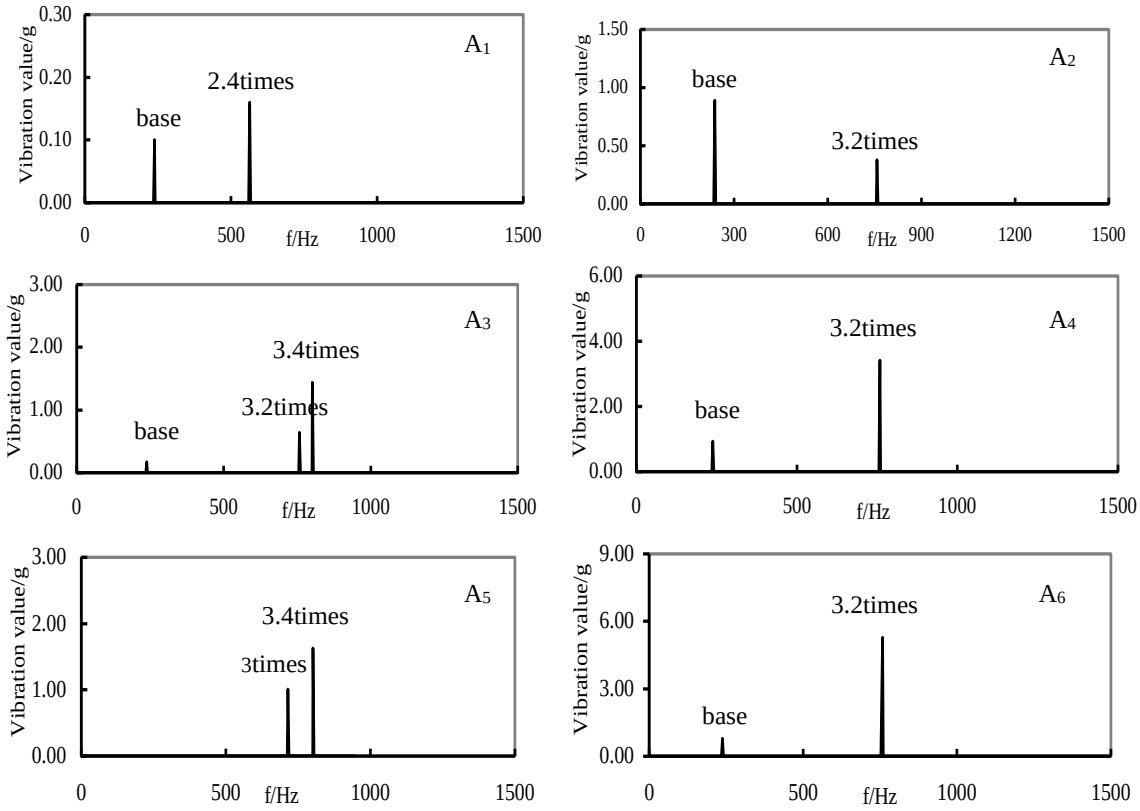

Figure 4 – Frequency spectrum of vibration acceleration of support at 40 percent rated working speed (fault state).

3.2 Fault Analysis

This study analyzed the joint pattern between the two low-pressure turbine simulated disks and joint structure between the two low-pressure turbine simulated disks and low-pressure shaft. The two low-pressure turbine simulated disks were centered by 6 locating pins, located by the mating face with only 1.2 mm in length. The join between the two disks and 6 locating pins was clearance fit. The first stage simulated disk of low-pressure turbine and low-pressure shaft were centered by 6 incomplete petal-shaped interfaces (incomplete cylindrical surface with only 1.5 mm in length). The second stage simulated disk of low-pressure turbine and low-pressure shaft were centered by the cylindrical surface. And the spline related to the torque transmission section. The complex structures of the low-pressure turbine simulated disks may lead to faults as the positioning of disks that ran at a high speed was unreliable. Schematic diagram of turbine structure is as shown in figure 5. As shown in figure 5, the No.1 locating surface was the mating surface between the first stage simulated disk of the low-pressure turbine and the low-pressure shaft, and the No.2 locating surface was the mating surface between the second stage simulated disk and the low-pressure shaft, the same as below.

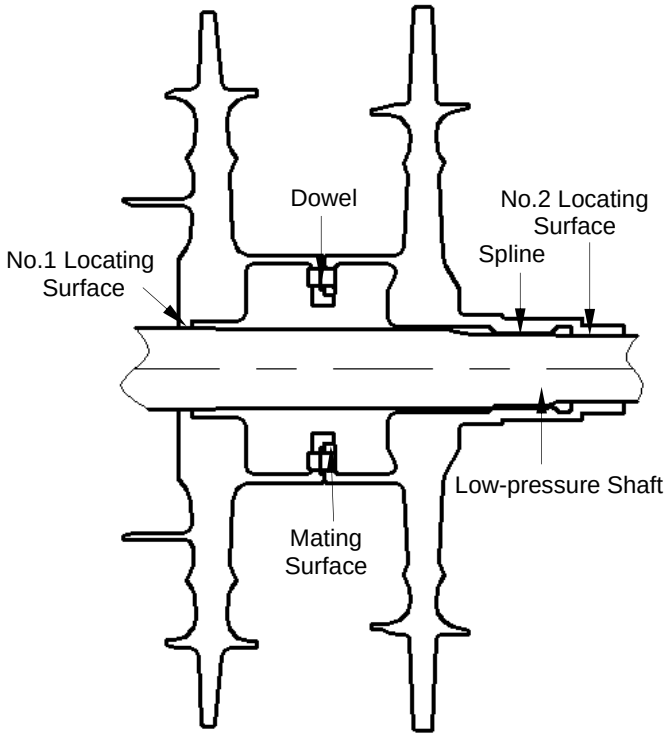

Figure 5 – Schematic diagram of turbine structure of the rotor.

3.3 Structure Improvement

To ensure the reliable positioning of the low-pressure turbine simulated disks that ran at a high speed and reduce the instable structure without changing the center of mass, mass and moment of inertia, improvement measures were put forward as follows. The two turbine simulated disks worked as a whole part and the 6 dowels were removed. The disks and the low-pressure shaft were improved with the cylindrical surface being the locating surface and splines providing the torque transmission. Also, under the analysis of dynamic characteristic calculation, the improved structure had no substantive impact on the dynamic characteristics of the rotor. The improved structure of the low-pressure turbine simulated disks is as shown in figure 6.

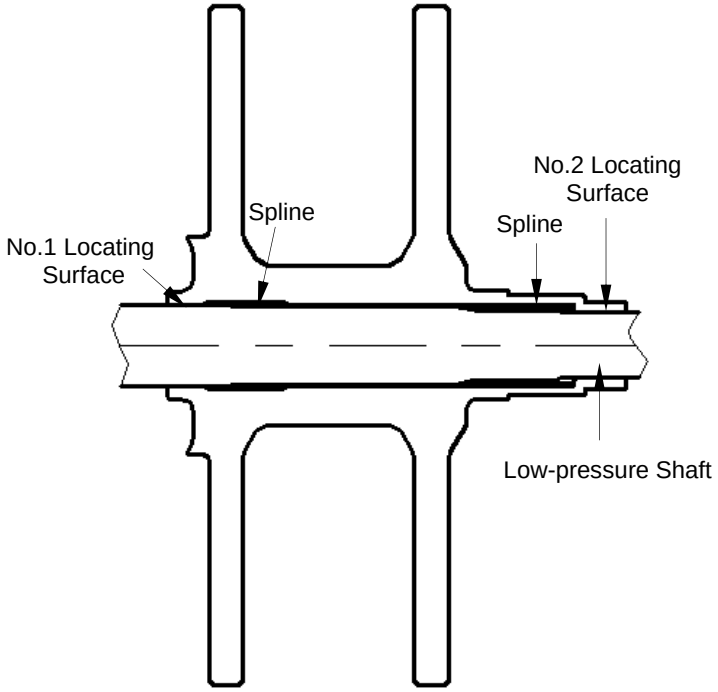

Figure 6 – Improved schematic diagram of turbine structure of the rotor.

4. Dynamic Characteristic Analysis

4.1 Finite Element Model

The dynamic characteristic calculation model of the simulated low-pressure rotor was established by finite method. The model was established by SAMCEF/ROTOR software. The main body and support of rotor were simulated by beam element and bearing element respectively, meanwhile, for the convenience of modeling, some fan simulation panels were simulated with lumped mass cells. The finite element model of the rotor is as shown in figure 7. In figure 7, the “O” represents concentrated mass.

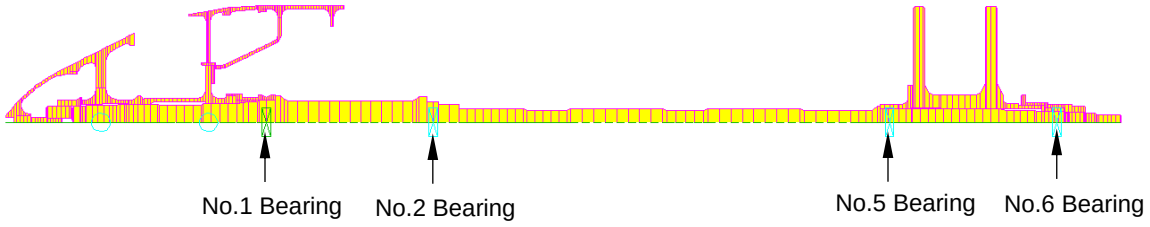

Figure 7 – The finite element model of the rotor.

4.2 Calculation Results of Critical Speeds and Mode Shapes

The supporting stiffness for calculation of each bearing is as shown in Table 1. The first three-stage critical speeds and mode shapes were calculated. The first three stages critical speeds and their margin were as shown in Table2. Besides, the first three-stage mode shapes were as shown in Figure8. The formula for calculating critical speed margin is as follows.

$$\textit{Critical speed margin}=[(|\textit{Working speed}-\textit{Critical speed})/\textit{Working speed}]*100\% \quad (1)$$

Table1–The supporting stiffness for calculation.

Supporting number	NO.1	NO.2	NO.5	NO.6
Stiffness/(E+7N/m)	1.0	5	0.1	5

Table2 –The calculation results of the first three stages critical speeds and margin.

Stages	First	Second	Third
Critical speeds/(rpm)	9326	14620	54551
Margin/(%)	>70	>50	>50

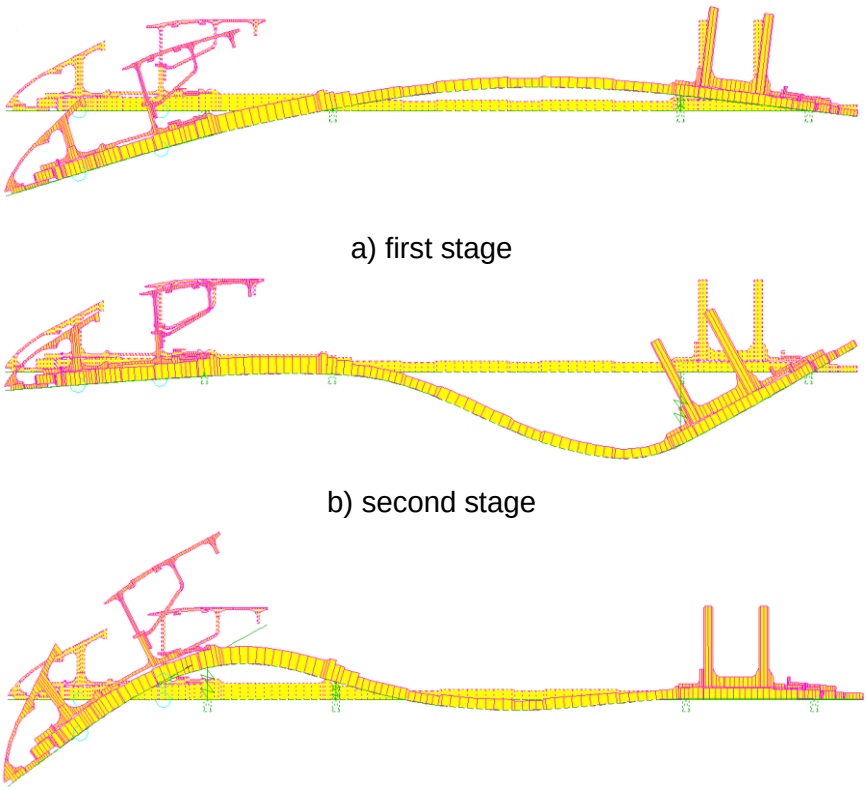

a) first stage

b) second stage

c) third stage

Figure 8 – The first three stages mode shapes of the rotor.

From table 2 and figure 8, it is known that the simulated low-pressure rotor worked above two critical speeds, and the first three stages critical speed margin were greater than 50%, which meets the critical speed design criteria [16]. Besides, the first three mode shapes of the rotor were all flexural mode shapes, and the spindling of the low-pressure shaft was the main cause of the bending deformation of the rotor.

5. Test Verification

5.1 Test Results

Dynamic characteristic experiments were carried out on the rotor with improved the low-pressure turbine simulated disks. The results showed that the simulated low-pressure rotor could steadily reach every level of the critical speed, operate to the rated working speed and its vibration performance was good at full speed range. Figure 9 shows the vibration amplitude speed curve measured by four displacement sensors in the full speed range. In figure 9, the relative speed is defined as follows.

$$relative\ speed = (actual\ speed / rated\ working\ speed) * 100\% \quad (2)$$

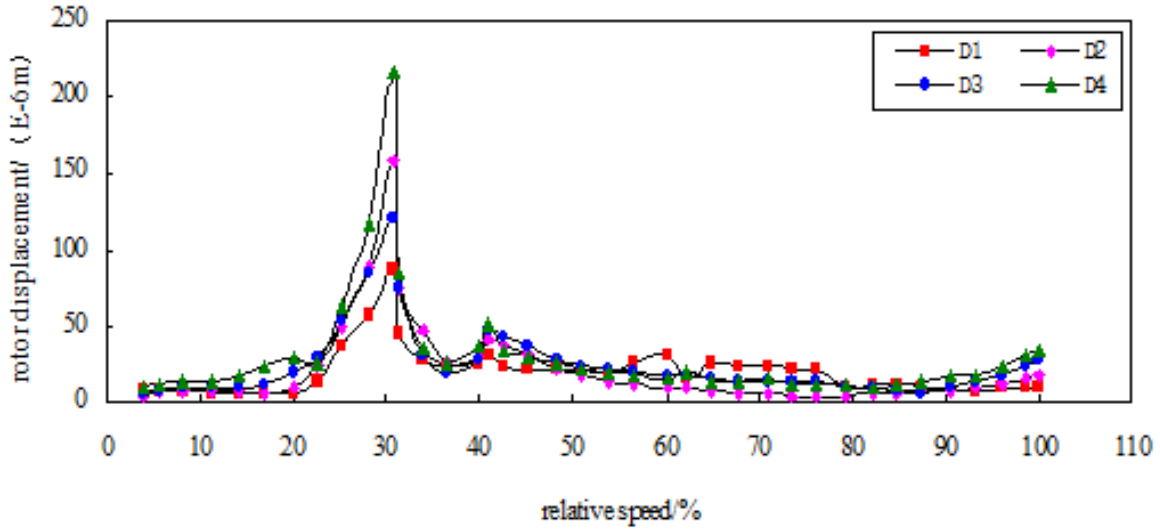

Figure 9 –The displacement-speed curve of the rotor in the whole speed range measured by four displacement sensors.

The spectrum diagram of the simulated low-pressure rotor at 40 percent rated working speed is shown in figure 10. Before and after improving the simulated low-pressure turbine, the total value of the vibration acceleration of each pedestal at 40 percent rated working speed is shown in table 3.

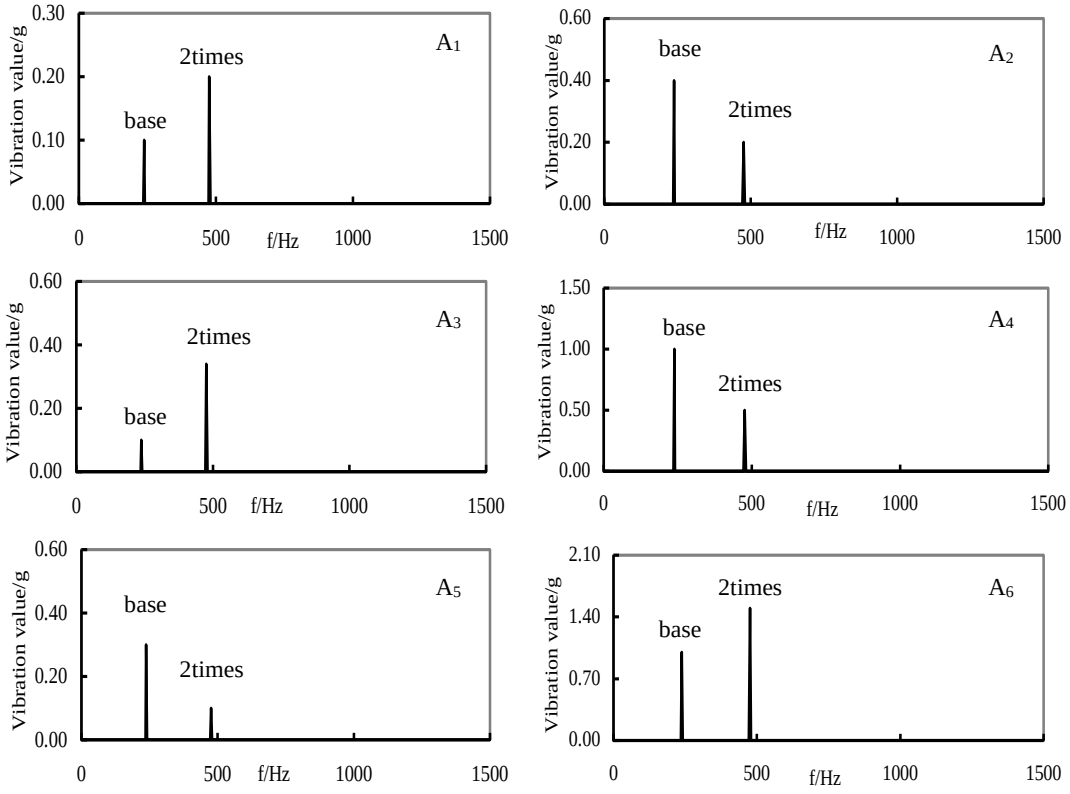

Figure 10 – Frequency spectrum of vibration acceleration of support at 40 percent rated working speed (after improving low- pressure turbine simulated disk's structure).

Table3 – Comparison of total value of vibration acceleration at 40 percent rated working speed.

Sensor	A_1	A_2	A_3	A_4	A_5	A_6
Total value before improving/(g)	0.69	0.83	1.63	3.58	1.88	5.80
Total value after improving/(g)	0.35	0.52	0.89	1.65	0.56	2.41

It can be seen from figure9, figure10 and table3 that after adopting the improved structure, the simulated low-pressure rotor can safely operate to the rated working speed, the vibration characteristics were good in the whole test process, and the total value of vibration acceleration of each pedestal was greatly reduced compared with that before the improvement, the reduction was no less than 37.35 percent, the frequency component of vibration acceleration of each pedestal was "clean", which there was non-integer frequency component.

The simulated low-pressure rotor could steadily reach every level of the critical speed, operate to the rated working speed and its vibration performance was good at full speed range. The results of the spectrum analysis showed that non-integer frequency component no longer existed when the rotor running at 40 percent rated working speed.

5.2 Calculation Analysis

According to the test results, the test values and calculation errors of the first two stages critical speeds of the simulated low-pressure rotor were obtained, which is as shown in Table 4. The calculation error is defined as follows:

$$Calculation\ errors=[(|test\ result-calculated\ result|)/test\ result]*100\% \quad (3)$$

Table4 – Comparison between the calculated results and the test results of the first two stages critical speeds.

Critical speed Stages	First	Second
Calculated results/(rpm)	9326	14620
Test results/(rpm)	9657	14501
errors/(%)	3.42	0.82

It is known from table4 that the error of the first order speed calculation is 3.42%, and the critical error of the second critical speed is 0.82%. Considering the difference of the actual complex structure and stiffness of the rotor, the calculation results were in good agreement with the test results. The finite element model established well reflected the actual dynamic characteristics of the simulated low-pressure rotor.

6. Conclusion

In this paper, the fault analysis and dynamic characteristics of a simulated low-pressure rotor with complex structure of a small turbofan engine were studied. Dynamic characteristic experiments were carried out on the rotor with improved the low-pressure turbine simulated disks. The rotor could steadily reach every level of the critical speed, operate to the rated working speed and its vibration performance was good at full speed range. The main conclusions are as follows:

(1) In the process of structural design of the complex structure rotor in aeroengine, attention should be paid to the positioning reliability of the connecting parts of the main parts. And the intermediate connecting structure with unreliable positioning should be avoided.

(2) The improvement measures were effective and the fault location was accurate. The vibration characteristics of the simulated low-pressure rotor in the whole speed range were good after adopting the improved measures, which verified the rationality of the whole rotor structure.

(3) The finite element model established well reflected the actual dynamic characteristics of the simulated low-pressure rotor.

(4) The result can provide references for the structural design of low-pressure rotor.

7. Contact Author Email Address

Mailto: nwjxj@126.com.

8. Copyright Statement

References

[1] WU Guofan, CHEN Guozhi and TU Mengpi. Analysis and experimental study of the high speed flexible rotor dynamic behaviors. *Journal of Aerospace Power*, Vol. 26, No. 3, pp563- 568,2006.

[2] DENG Wangqun, WANG Yi, NIE Weijian, HE Ping and XU Youliang. Influence Analysis of Supporting Stiffness and Supporting Axial Location on Critical Speeds of a Low-pressure Rotor of a Counter Rotating Engine. *Aeroengine*, Vol. 42, No. 3, pp7-11, 2016.

[3] LIU Yang, TAI Xingyu, ZHAO Qian and WEN Bangchun. Dynamic Characteristics of Misalignment-Rubbing Coupling Fault for Rotor System. *Journal of Northeastern Univerisity(Natural Science)*, Vol. 34, No.4, pp 564-568, 2013.

[4] XU Qi, WU Hao, ZHAO Lichao, YAO Hongliang and WEN Bangchun. Quantitative coupling fault diagnosis method of multi-span rotor based on harmonic components.*Journal of Vibration Engineering*, Vol. 28, No.3, pp 495-502, 2015.

[5] DENG Wangqun, NIE Weijian, XU Youliang, YUAN Sheng and LIU Wenkui. Vibration fault analysis and balance technique study of a high speed flexible rotor of a turbofan engine. *Gas Turbine Experiment and Research*, Vol. 31, No. 1, pp 24-30,58,2018.

[6] GAO Feng. The Vibration Fault Analysis of Aero Engine High Pressure Rotor[D]. Tianjin: Civil Aviation University of China,2015.

[7] LIU Jianxiong. Study on Typical Vibration Fault Mechanism Modeling and Response Characteristics of Certain Aero Engine Rotor System[D]. Wuhan: Huazhong University of Science and Technology,2015.

[8] HUANG Guoyuan. Numerical Simulation and Experiment Research on Rotor System with Unbalance-Misalignment-Rubbing Multi-Faults[D]. Nanjing: University of Aeronautics and Astronautics,2018.